Extended object tunneling: Current-carrying states of Abrikosov vortices in a superconductor with artificial nanobarriers

B. Rosenstein,[1,2] I. Shapiro,[3] B. Ya. Shapiro,[3] Dingping Li,[4] A. Frydman,[3] S. Poran,[3] and D. Berco[2]

[1]*Department of Electrophysics, National Chiao Tung University, Hsinchu, Taiwan, R.O.C.*

[2]*Applied Physics Department, Ariel University Center of Samaria, Ariel IL-40700, Israel*

[3]*Department of Physics, Institute of Superconductivity, Bar-Ilan University, IL-52900 Ramat-Gan, Israel*

[4]*Department of Physics, Peking University, Beijing 100871, China*

(Received 27 January 2012; published 24 February 2012)

We consider the structure and dynamics of two-dimensional fluxons created by a magnetic field in a type-II superconductor film with critical temperature T_1 in the presence of nanostripes of material with a higher critical temperature T_2. The width of the stripes is of the order of the coherence length ξ. Such a stripe plays the role of a potential barrier for vortices. When subjected to the current J parallel to the stripe, vortices move toward the barrier. Below the critical current J_c, the flux flow is effectively halted by the barrier, while above J_c, flux penetrates the stripe and passes the barrier. The mechanism of the barrier penetration ("soliton tunneling" occurs even at zero temperature) is rather unusual: the vortices adjust their shape, and upon passing the barrier, they shrink their cores. The critical current and the I-V curves are calculated numerically and analytically using variational approach.

DOI: 10.1103/PhysRevB.85.054512 PACS number(s): 74.20.De, 74.25.Wx, 74.25.Sv

I. INTRODUCTION

A magnetic field penetrates a type-II superconductor in the form of vortices with the superconducting order parameter suppressed at the centers, thereby creating an inhomogeneity.[1] Its value is recovered to the bulk value only a distance (of the order of the coherence length ξ) away from the core, while the distribution of the magnetic field varies on a typically much larger scale of the magnetic penetration depth λ. In the interesting case of strongly type-II superconductor or films (even made of type-I superconductors), λ is much larger than ξ. Fluxons are spatially extended objects that are topologically stable, can move under influence of the bias current, and interact with defects and with each other. The great interest in the problem of magnetic flux pinning is caused by both the technological applications and rich basic physics associated with nonlinear flux dynamics.[2,3] It is well known that in magnetic fields, the zero-resistance property of the superconductors is lost due to the dissipative motion of the magnetic fluxons (Abrikosov vortices) in the form of flux flow or creep. In order to restore the superconductivity, one has to find an efficient way to stop the flux flow by "pinning" the vortices. An important challenge in applications of type-II superconductors is achieving optimal critical currents $J_c(B)$ under an applied magnetic induction H. The electric current acts as a driving force on the vortex matter, and there is an intricate interplay between the stress and the elasticity of the vortex matter and the pinning strength. The phase boundary between the static phase and a moving (flux flow or creep) phase is determined by the critical current as a function of parameters of the system: magnetic field, temperature, and pinning strength. The available magnetic field, especially in high-temperature superconducting materials, becomes increasingly large. Unfortunately, the critical current decreases as magnetic induction B grows. Consequently, optimization of the pinning efficiency becomes a central issue for applications.

Although intrinsic pinning always exists in bulk superconductors, it is rather inefficient especially at elevated fields. Recently, a new way, i.e., pinning by artificially assembled arrays of pointlike "pinning centers," has been developed. In this case, the pinning center is a region where superconductivity is suppressed compared to the bulk by a variety of techniques (particle irradiation,[4] lithography,[5] laser irradiation[6]). The suppression can be described as a reduced (sometimes to zero) local critical temperature T_2 compared to that of the bulk T_1. The basic idea therefore hinges on creation of "defects" or potential wells to *attract* vortices. There are two important disadvantages of this method. Evidently, the sample is damaged by the number of defects required especially at large magnetic fields and, in addition, it is very difficult to ensure that vortices can not sneak around the pointlike structures.[7]

In this paper, we propose an alternative to achieve a stable controllable flux pinning in thin films that is effective at large magnetic fields. To simplify the discussion, let us consider a sufficiently thin film where the vortices can be considered two dimensional (2D) (generalization to thick samples is straightforward). The main idea is that instead of considering *attracting pointlike*[zero-dimensional (0D)] structures, one can use *repelling lines* [one dimensional (1D)] crossing the sample, thus effectively blocking the vortex motion (see Fig. 1). To repel vortices, this stripe should be made from a *better* superconductor with the critical temperature T_2 exceeding that of the bulk T_1. In this case, one avoids damaging the sample, while vortices can not topologically sidestep the repelling lines. Formally, the repelling stripe acts as an extended two-dimensional object, a barrier, for a system of vortices driven by the Lorentz force of the bias current. The critical current in this case is determined by the ability of the vortices to "tunnel" through the barrier. The barriers should not be much wider than ξ to prevent the fluxon creation inside the barrier.

The vortex passage process becomes very unusual and complicated since the vortices can not be considered pointlike objects. At barrier width comparable with the vortex core size, the core-shape degrees of freedom play a major role.

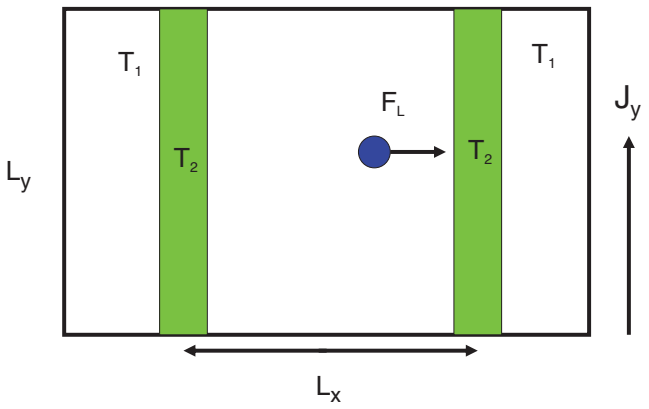

FIG. 1. (Color online) Vortex dynamics in the presence of a barrier. A segment of size $L_x \times L_y$ of a type-II superconducting film made from material with the critical temperature T_1 is subjected to a perpendicular magnetic field $\mathbf{H} = H\hat{\mathbf{z}}$ and the transport current $\mathbf{J} = J\hat{\mathbf{y}}$. The barrier is a superconductor with higher critical temperature $T_2 > T_1$. The sample is periodic with period L_x. Abrikosov vortices are driven by the Lorentz force F_L and are repelled by the stripe.

Mathematically, the vortex core structure is described by the distribution of the superfluid density (vanishing at the center of the vortex). One therefore arrives at the theoretically challenging question of dynamics of a soliton moving through a potential varying on the scale of the soliton size. This was an additional motivation for our study.

Theoretically, the problem of tunneling of the extended object (the soliton) through the barrier is therefore considerably different from that of motion of a vortex line near a two-dimensional defect, extensively studied in connection with twinning planes in high-T_c materials[2,8] for which the core structure is unimportant. The main phenomenon that attracted attention was the curving (creation of loops) of the vortices along the vortex axis (approximately the field direction) and in-plane dynamics. These effects are unimportant in the case of thin films, intensively studied experimentally nowadays. This case will be mainly addressed in this paper. In this case, the system is essentially two dimensional. The 2D problem of single-vortex tunneling through a thin barrier (of order of Thomas-Fermi screening length smaller than ξ) of a special form was studied early on in connection with an idea of increasing critical current by an applied electric field effect.[9,10] Even for a single-vortex system, it was noticed that the relevant feature of the pinning process is the vortex core structure rather than the distribution of the magnetic field. The critical current was calculated from stability analysis of static configurations of the superconducting order parameter (assuming a round 2D Abrikosov vortex). When the bias current exceeds the critical value J_c, the vortex system loses stability, vortices penetrate the barriers, and flux flow ensues. The dynamics of the vortex passing a barrier, however, has not been considered. As was observed in recent simulations,[11] this is expected to be quite intricate. Just above the depinning, strong inhomogeneous electric fields appear and vortex cores get deformed. Even deep in the flux flow regime, the shape of the vortex core is modified.[12]

In this paper, the critical current, local electric field distribution at depinning, and the voltage-current characteristics are calculated numerically and analyzed analytically in the framework of the simplified time-dependent Ginzburg-Landau approach (GL) appropriate for large magnetic fields.[3,11] The process of vortices tunneling through the barrier above the critical current was studied in detail, and it was found that the passage through a narrow barrier (compared with the vortex core size of the order of the coherence length ξ) indeed is accompanied by a significant vortex-shape change.

The paper is organized as follows. A general GL setup including effects of the electric field in dynamics is briefly described in Sec. II. A description of the numerical method and results for different barrier width and driving currents are presented in Sec. III for both static and dynamics current-carrying states. In Sec. IV, an analytical theory of the pinned states and critical current is developed for arbitrary shape of the barrier and compared with numerical results. Summary and discussion are the subjects of the concluding Sec. V.

II. VORTEX DYNAMICS OF TYPE-II SUPERCONDUCTORS IN A STRONG MAGNETIC FIELD

Pinning of a vortex is determined by properties of its core (which is of the size of ξ); the distribution of the order parameter becomes of importance. Since a microscopic theory in the inhomogeneous situation is not practical, the only available tool is the Ginzburg-Landau phenomenological approach.[1] Static magnetic properties of the superconductor are described by the GL Gibbs energy as function of the order parameter Ψ and vector potential $\mathbf{A}$:

$$F_{\rm GL}[\Psi,\mathbf{A}] = \int dz\, d\mathbf{r}\Big[\frac{\hbar^2}{2m_c^*}|\partial_z\Psi|^2 + \frac{\hbar^2}{2m^*}|\mathbf{D}\Psi|^2 - a'(\mathbf{r})|\Psi|^2 + \frac{b'}{2}|\Psi|^4 + \frac{1}{8\pi}(\mathbf{B}-\mathbf{H})^2\Big]. \quad (1)$$

$\mathbf{D} \equiv \nabla - i\frac{2\pi}{\Phi_0}\mathbf{A}$ denotes the covariant derivative and $\Phi_0 = \frac{hc}{e^*}$, $e^* = 2|e|$ is the unit of flux, $\mathbf{B} = \nabla \times \mathbf{A}$ is the magnetic induction. Here,

$$a'(\mathbf{r}) = \alpha[T_c(\mathbf{r}) - T]. \quad (2)$$

The simplest relaxation dynamics of a superconductor in the presence of an electric field is described by the time-dependent Ginzburg-Landau (TDGL) equation[1,3]

$$\frac{\hbar^2\gamma}{2m^*}D_t\Psi = -\frac{\delta}{\delta\Psi^*}F_{\rm GL}, \quad (3)$$

where scalar potential Φ appears in the electric field $\mathbf{E} = -\nabla\Phi - \frac{1}{c}\frac{\partial}{\partial t}\mathbf{A}$ and in the covariant time derivative $D_t \equiv \frac{\partial}{\partial t} - i\frac{e^*}{\hbar}\Phi$. The inverse diffusion constant γ in metals is simply related to the normal-state conductivity σ_n.[1] An external current J will be applied in the y direction, so that the vortices are moving along the x direction (see Fig. 1).

The approach simplifies considerably when the magnetic induction exceeds significantly the lower critical field $H_{c1}(T)$. The distribution of the magnetic induction becomes practically uniform, and the only dynamic degrees of freedom are the order parameter Ψ and the electric field E. We consider a superconducting slab of dimensions $L_x \times L_y \times L_z$ subjected to a sufficiently high, homogeneous, and time-independent magnetic induction perpendicular to the slab $\mathbf{B} = B\hat{\mathbf{z}}$. For

strongly type-II superconductors, the ratio of penetration depth to coherence length, $\kappa \equiv \lambda/\xi$, is very large. In thin films, this condition becomes $\lambda_{\rm eff}/\xi \gg 1$, and is almost satisfied since the penetration depth becomes $\lambda_{\rm eff} = 2\lambda^2/L_z$. The magnetization is smaller than the field by the factor $1/\kappa^2$ (Ref. 11) and, consequently, for magnetic fields a few times larger than H_{c1}, $B \approx H$ is practically homogeneous. Hence, the vector potential $\mathbf{A} = \mathbf{B} \times \mathbf{r}/2$ is not a dynamic variable. The same, however, can not be assumed for the electric field. Although far above the depinning transition the electric field is nearly homogeneous due to reasons similar to those that led to homogeneity of the magnetic field (see Ref. 12) and, as was shown in Ref. 7, it becomes highly inhomogeneous near the depinning point considered in this paper. Therefore, the scalar potential is a dynamic variable.

The system is invariant under translations in the field directions, so we use a 2D dimensionless energy density $f_{\rm GL}$:

$$F_{\rm GL} = \frac{H_{c2}^2}{8\pi\kappa^2} L_z \int d\mathbf{r}\, f_{\rm GL}. \tag{4}$$

In this paper, $\xi = \hbar/(2m^*\alpha T_c)^{1/2}$ will be used as a unit of length $\mathbf{r} \to \mathbf{r}/\xi$; $H_{c2} = \frac{\Phi_0}{2\pi\xi^2}$ as a unit of magnetic field, $b = B/H_{c2}$. The scaled order parameter is $\psi = \Psi/2^{1/2}\Psi_0$, where $|\Psi_0| = (\alpha T_1/b')^{1/2}$, so that the dimensionless energy density can be written in the form

$$f_{\rm GL} = -\frac{1}{2}\psi^* D^2\psi - \left[\frac{1-t}{2} + U(x)\right]\psi^*\psi + \frac{1}{2}(\psi^*\psi)^2, \tag{5}$$

where $t = T/T_1$ and a dimensionless "pinning" potential $U(\mathbf{r})$ is a trapezoidal, one-dimensional stripe sketched in Fig. 2:

$$U(x) = U_0 u(x), \tag{6}$$

where $U_0 = \frac{T_2 - T_1}{2T_1}$ is the strength of the potential that the vortex core "feels." The function $u(x) < 1$ describes the shape of the barrier: it approaches 1 inside the better superconductor with critical temperature T_2, and approaches zero in the bulk superconductor with the lower critical temperature T_1. In numerical simulations, we use a Gaussian

$$u(x) = \exp(-x^2/2w^2). \tag{7}$$

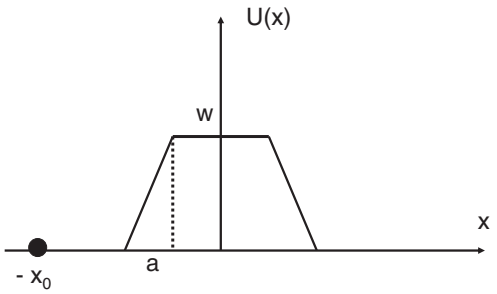

FIG. 2. Geometry of the potential barrier for the Abrikosov vortices. Width of the stripe is w, while a is the width of the interface between the stripe and the bulk superconductors. Position of the vortex center (where the order parameter vanishes) is indicated by x_p.

The potential barrier is assumed to be repeated periodically with period L_x (in simulations implemented by periodic boundary conditions).

In analogy to the coherence length, one can define a characteristic time scale. In the superconducting phase that is a typical "relaxation" time $t_{\rm GL} = \gamma\xi^2/2$, leading in our case to the time-dependent equation

$$\begin{aligned} D_t\psi &= -\frac{\delta}{\delta\psi^*} f_{\rm GL}[\psi] \\ &= -\frac{1}{2}D^2\psi - \left[\frac{1}{2}(1-t) + U(x)\right]\psi + \psi^*\psi^2, \end{aligned} \tag{8}$$

where $D_t = \partial_t + i\phi$ is utilizing the dimensionless scalar potential. In our gauge, the dimensionless electric field $\mathcal{E} = E/E_{\rm GL} = -\nabla\phi$, where unit of electric field is $E_{\rm GL} = H_{c2}\frac{\xi}{ct_{\rm GL}}$. Equation (8) is supplemented (neglecting time variations of the charge density that occur on the atomic scale) by the charge conservation law[1] $\nabla \cdot \mathbf{J} = 0$, where the current density consists of two parts

$$\mathbf{J} = \frac{ie^*\hbar}{2m^*}(\Psi^*\mathbf{D}\Psi - \Psi\mathbf{D}\Psi^*) + \sigma_n\mathbf{E} = J_d\mathbf{j} \tag{9}$$

in the units of the depairing current

$$J_d = \frac{cH_{c2}}{2\pi\xi\kappa^2}. \tag{10}$$

Therefore, the dimensionless current density, including the normal component, is given in our gauge by

$$\mathbf{j} = \frac{i}{2}[\psi^*\mathbf{D}\psi - \psi(\mathbf{D}\psi)^*] - k\nabla\phi, \tag{11}$$

where the conductivity will be given in units of

$$\sigma_{\rm GL} = \frac{c^2 t_{\rm GL}}{2\pi\lambda^2} = \frac{c^2\gamma}{4\pi\kappa^2}. \tag{12}$$

This unit is close to the normal-state conductivity in low-T_c superconducting metals in the dirty limit $\sigma_n = \frac{c^2\gamma}{8\pi\kappa^2}$[1]. More generally, there is a factor $k$of order 1, $\sigma_n = k\sigma_{\rm GL}$. Therefore, the second equation is

$$k\nabla^2\phi = \frac{i}{2}\nabla[\psi^*\mathbf{D}\psi - \psi(\mathbf{D}\psi)^*]. \tag{13}$$

The system of equations should be complemented by the following metallic electrodes boundary conditions in the y direction:

$$-\nabla_y\phi = j^{\rm ext}|_{y=0,L_y}, \quad \nabla_x\phi = 0|_{y=0,L_y}, \quad \psi = 0|_{y=0,L_y}. \tag{14}$$

Periodic boundary conditions in the x direction (with period L_x) are assumed and periodic under magnetic translations[7] in the x direction. This system of equations is solved numerically after appropriate discretization in both static and dynamic situations in the next section and analyzed analytically in Sec. IV (only in a stationary current-carrying state) using exact relations between space averages of physical quantities derived from the GL equations.

III. NUMERICAL SOLUTION OF THE TDGL EQUATIONS

A. Discretized form of the electrodynamics

The above equations were treated numerically using Wilson's discretization (see details in Refs. 7,13). The points on the grid (in units of ξ) $\mathbf{r_n} = (n_1 a_x, n_2 a_y)$ are labeled by two integers $n_1 = 1, \ldots, n_{\max}$ and $n_2 = 0, \ldots, n_{\max}$. The grid lattice spacings are $a_x^2 = \frac{4\pi}{\sqrt{3} b s^2}$ and $a_y^2 = \frac{\sqrt{3}\pi}{b s^2}$, where s is an integer. Our sample has the aspect ratio of $\frac{L_y}{L_x} = \frac{\sqrt{3}}{2}$ with $n_{\max} = s N^{1/2}$, so that number of vortices between two barriers is N.

The constant homogeneous magnetic field is described by the Wilson link phases $\exp(i\theta^{\gamma}_{n_1,n_2})$:

$$\theta^1_{n_1,n_2} = -\frac{\pi}{s^2} n_2, \quad \theta^2_{n_1,n_2} = \frac{\pi}{s^2} n_1. \tag{15}$$

Periodic (magnetic) boundary conditions for the rectangular sample read as

$$\begin{aligned} \psi_{0,n_2} &= \exp\left[i \frac{\pi n_{\max}}{s^2} n_2 \right] \psi_{n_{\max},n_2}, \\ \psi_{n_{\max}+1,n_2} &= \exp\left[-i \frac{\pi n_{\max}}{s^2} n_2 \right] \psi_{1,n_2}, \\ \psi_{n_1,0} &= 0, \quad \psi_{n_1,n_{\max}} = 0. \end{aligned} \tag{16}$$

The corresponding boundary conditions for the scalar potential are

$$\begin{aligned} \phi_{0,n_2} &= \phi_{n_{\max},n_2}, \quad \phi_{n_1,0} = \phi_{n_1,n_{\max}}, \\ \phi_{n_1+1,0} - \phi_{n_1,0} &= \phi_{n_1+1,n_{\max}} - \phi_{n_1,n_{\max}0} = \phi(0,0,0) = 0, \\ \frac{1}{a_y}(\phi_{n_1,1} - \phi_{n_1,0}) &= -j^{\text{ext}}, \\ \frac{1}{a_y}(\phi_{n_1,n_{\max}} - \phi_{n_1,n_{\max}-1}) &= -j^{\text{ext}}, \\ \phi_{n_1+1,0} - \phi_{n_1,0} &= \phi_{n_1+1,n_{\max}} - \phi_{n_1,n_{\max}} = 0. \end{aligned} \tag{17}$$

The discretized TDGL equations are

$$\begin{aligned} &\frac{\psi_{n_1,n_2}(\tau + \Delta\tau) - \psi_{n_1,n_2}(\tau)}{\Delta\tau} \\ &= i\phi_{n_1 n_2} \psi_{n_1,n_2} + \frac{s^2 b\sqrt{3}}{8\pi} K_{n_1,n_2} \\ &\quad + \left(\frac{1-t}{2} + U_{n_1} \right) \psi_{n_1,n_2} - |\psi_{n_1,n_2}|^2 \psi_{n_1,n_2}, \end{aligned} \tag{18}$$

where

$$\begin{aligned} K_{n_1,n_2} = \big[&\exp\left(i\theta^1_{n_1,n_2}\right) \psi_{n_1+1,n_2} + \tfrac{4}{3} \exp\left(i\theta^2_{n_1,n_2}\right) \psi_{n_1,n_2+1} \\ &+ \exp\left(-i\theta^1_{n_1-1,n_2}\right) \psi_{n_1-1,n_2} \\ &+ \tfrac{4}{3} \exp\left(-i\theta^2_{n_1,n_2-1}\right) \psi_{n_1,n_2-1} - \tfrac{14}{3} \psi_{n_1,n_2} \big]. \end{aligned}$$

The barrier is described by a discretized smoothed-out form of Eq. (6):

$$U_{n_1} = U \exp\left[-\frac{(a_x n_1)^2}{2w^2} \right], \tag{19}$$

where the width w is also the distance between the center and the location of the largest derivative force. The discretized Poisson equation (13) reads as

$$\begin{aligned} k \Bigg[&\frac{\phi_{n_1-1,n_2} - 2\phi_{n_1,n_2} + \phi_{n_1+1,n_2}}{a_x^2} \\ &+ \frac{\phi_{n_1,n_2-1} - 2\phi_{n_1,n_2} + \phi_{n_1,n_2+1}}{a_y^2} \Bigg] \\ &= i \frac{s^2 b\sqrt{3}}{8\pi} \psi^*_{n_1,n_2} K_{n_1,n_2} + \text{c.c.} \end{aligned} \tag{20}$$

The supercurrent density is discretized as

$$j^{s2}_{n_1,n_2} = \frac{i}{2a_y} \psi^*_{n_1,n_2} \exp\left(i\theta^2_{n_1,n_2}\right) \psi_{n_1,n_2+1} + \text{c.c.} \tag{21}$$

B. Numerical method

The numerical method utilized is a combination of the Crang-Nicholson algorithm for the TDGL equation (18), with use of tridiagonal matrix algorithm (TDMA) for the Poisson equation (20) at each time step. The initial condition was set by the Abrikosov analytic expression.[14] As was discussed in Ref. 7, it has a number of advantages (including better stability) over the often-used fast Fourier transform. Evolution in time settled after several thousands of time steps of order $\Delta\tau = 2.5 \times 10^{-4} t_{\text{GL}}$. The magnetic field is taken as $b = 0.5$, the value of the normal-state conductivity in Eq. (12) with $k = 1$ and the temperature $t = 0$ was constant throughout our simulations. Variation of these parameters does not change qualitatively the results of our study. No thermal fluctuations on the mesoscopic scale were introduced, although an insignificant grid noise was present. We always used $s = 16$ corresponding to 16×16 grid points per vortex. The number of vortices was always quite large, $16 \times 16 = 256$ and $32 \times 32 = 1024$, to overcome boundary effects. This allowed us to check the scaling with L_x (see Sec. IV). In the middle of our sample (in the current direction y), the dynamics is independent of the edge effects due to the metallic leads. These effects are interesting in their own right, but in our figures we show the central area containing several vortices only. Now, we proceed to the description of the results for structures of pinned vortex matter and dynamics of the flux flow through the stripes for various barriers and transport currents.

C. Structure of the pinned current-carrying vortex state below the critical current

We start with statics. In Fig. 3, we show the distribution of the order parameter $|\psi|$ over a segment containing 16×16 vortices for $b = 0.5$ (in units of H_{c2}), interacting with a narrow Gaussian barrier [Eq. (19)] of width $w = 0.3\xi$ and strength $U_0 = (T_2 - T_1)/2T_1 = 1$ (thus corresponding to $T_2/T_1 = 3$). The external current density was set to be $j = 0.90 \times 10^{-3}$ (in units of the depairing current), just below the critical $j_c = 0.91 \times 10^{-3}$. Contours of the order parameter demonstrate that the barrier is sufficiently small, so that the structure of the single-vortex core is basically the same as that of the static lattice [Fig. 3(b)] calculated in Sec. IV B. However, the Gaussian barrier marked by lines at distances $\pm w$ causes

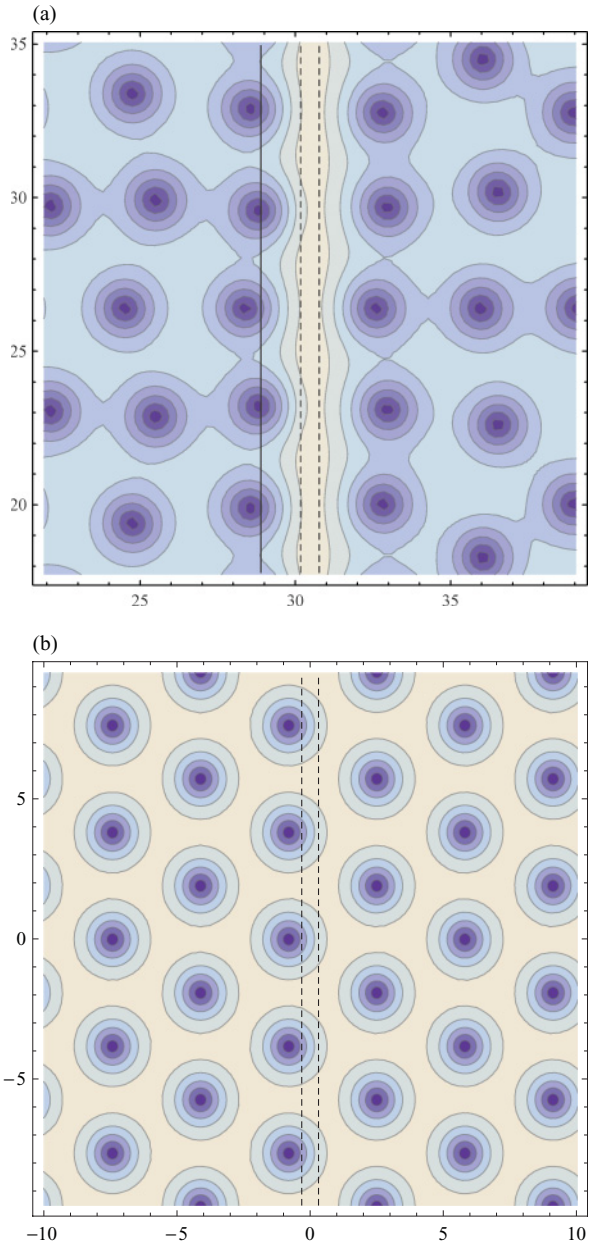

FIG. 3. (Color online) Numerical simulation of the 16×16 vortex system at magnetic field $b = 0.5$ in the presence of a stripe of superconductor with higher critical temperature compared to the static unperturbed Abrikosov lattice. Vortex matter is described by the contours of the superconducting order parameter $|\psi|$. The dashed lines mark the location of the narrow (width $w = 0.3$) Gaussian barrier given by Eq. (19) (a superconducting stripe with higher T_c) with strength $U_0 = 1$. (a) Current density $j = 0.9 \times 10^{-3}$ just below the critical one $j_c = 0.91 \times 10^{-3}$, in units of the depairing current [Eq. (10)]. Vortices in the bulk are arrested at certain distance x_p before the barrier (solid line), while less dense vortex matter inside the barriers is also immobile. Only the central part of the sample containing a few fluxons is shown. One observes that the vortex cores are still roughly round as in the Abrikosov lattice. The hexagonal symmetry is distorted by the barrier and becomes rectangular. (b) Unperturbed Abrikosov lattice [Eq. (36)] for the same value of parameters calculated analytically to next to leading order in small parameter $(1 - b)/2 = 0.25$ [see Eq. (36)].

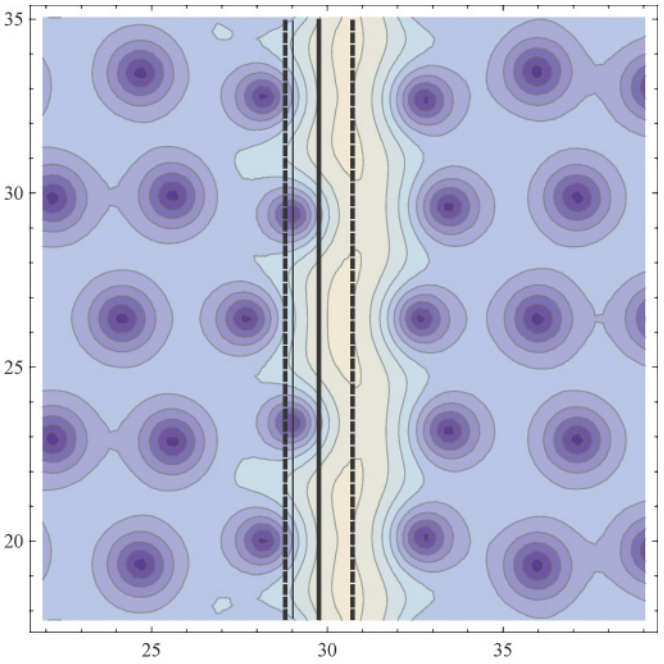

FIG. 4. (Color online) Static configuration of the order parameter for a wide stripe $w = 1.3$. Current density $j = 1.1 \times 10^{-3}$ below the critical current $j_c = 1.3 \times 10^{-3}$ for that barrier. Magnetic field and critical temperatures are as before ($b = 0.5$, $U_0 = 1$). One observes that the shape of vortex cores is still roughly round as in the Abrikosov lattice, however, the density of pinned vortices in front of the barriers is higher than in the bulk and there is an empty region behind the barrier. Moreover, near the barrier, the vortices are significantly smaller.

great enhancement of the order parameter there and the pinned lattice prefers a rectangular lattice for not very large distances between parallel barriers L_x.

In Fig. 4, the distribution of the order parameter for a rather wide, $w = 1.3\xi$, Gaussian barrier of the same strength and field is given at current $j = 1.1 \times 10^{-3}$ below the critical current $j_c = 1.3 \times 10^{-3}$ for that barrier. Vortices in the bulk are arrested at a certain distance $x_p(j)$ before the barrier (marked by a thin line). One observes that the vortex cores are still roughly round as in an Abrikosov lattice, however, the density of pinned vortices in front of the barriers is higher than in the bulk and there is an empty region behind the barrier. Moreover, near the barrier, the vortices are significantly smaller (see Fig. 4). The distribution of the order parameter as a function of distance from the vortex core can be approximated as

$$|\psi(\mathbf{r})| = \sqrt{\frac{1-b}{2\beta_A}}\tanh(\varepsilon r), \tag{22}$$

where the fitting parameter $\varepsilon > 1$ describes the compression of the vortex core and $\beta_A = 1.16$. In an undistorted Abrikosov lattice [see Eq. (36)], one gets a periodic array of cores with $\varepsilon = 1.37b^{1/2}$. This can be used only when b is not very small when the cores overlap. For the simulated value $b = 0.5$, it describes reasonably well large vortex cores far from the barrier in Fig. 4 ($\varepsilon \approx 1$). At fields much smaller than H_{c2}, the vortices become well separated and $\varepsilon = 1$. In the present case, one can fit the

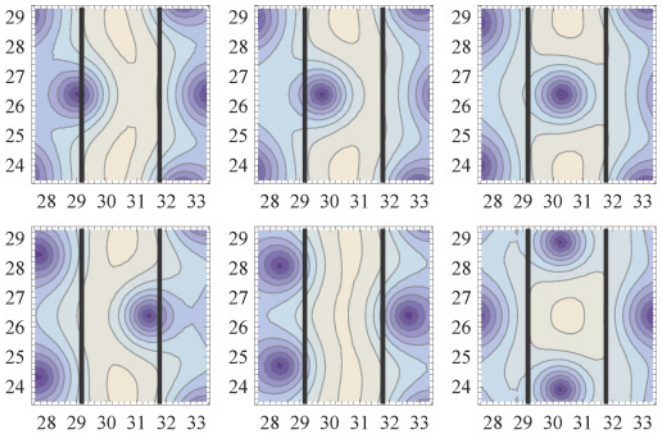

FIG. 5. (Color online) Dynamics of the barrier passage. At large current density, $j = 5.0 \times 10^{-3}$ in units of depairing current (above $j_c = 1.3 \times 10^{-3}$), vortices are able to penetrate the interface and therefore are bound to path the barrier. Six consecutive moments $t/t_{\rm GL} = 2100, 2200, 2240, 2280, 2400, 2740$ describe the passage of the vortices through the barrier. During the passage, the vortices become elongated. Parameters are the same as in Fig. 4.

core width of the pinned vortices by $\varepsilon = 3$. The case of pinning by a wide barrier is discussed analytically in Sec. IV D using the single-vortex model.

D. Vortex dynamics at interface between two superconductors and the critical current

The dynamics of a segment containing 16×16 vortices for $b = 0.5$ interacting with a rather wide, $w = 1.3\xi$, Gaussian barrier of strength $U_0 = 1$ is shown in Fig. 5. The steady-state evolution of the vortex system (after an initial transitional state of order of hundreds of $t_{\rm GL} = \gamma\xi^2/2$) at the current density $j = 5.0 \times 10^{-3}$ (above the critical current of $j_c = 1.3 \times 10^{-3}$) is shown by the contours of the superfluid density in dimensionless units of Sec. II. During five consecutive moments $t/t_{\rm GL} = 1000, 1100, 1140, 1180, 1240$, the vortices are able to penetrate the interface and therefore are bound to pass a wide barrier. However, the next passage of line of barriers takes a lot of time since the next passage occurs at

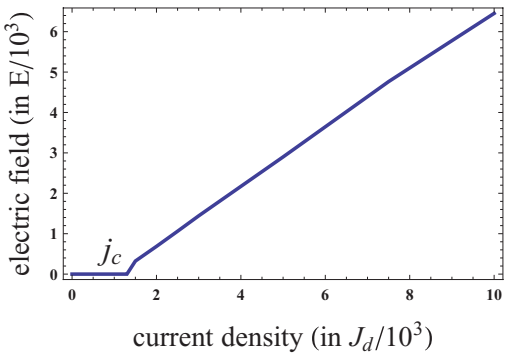

FIG. 6. (Color online) The dc I-V curve for the wide barrier. The Bardeen-Stephen law is shown by a straight line for comparison. The critical current is quite high, $j_c = 1.3 \times 10^{-3}$.

$t = 1700$, so that average velocity of the vortices is given by j. During this stage, the vortices repel each other moving along the barrier. Then, the process of fast passage starts again.

The I-V characteristics are given in Fig. 6 and demonstrate a linear Bardeen-Stephen behavior above j_c. Above the critical current, very large gradients of the electric field accompany the entrance of the vortices into the stripe as was observed in pinning situations.[7] The vortex lattice is rigid and rows of vortices enter simultaneously the barrier. Entrance of a line of vortices causes a spike in the electric field. These results are independent of the system size (as is demonstrated by comparison of part of the data with the larger sample size $L_x \times L_y = 32 \times 32$). Although the dynamics can be studied at present only numerically, the critical current can be estimated analytically quite well for a variety of situations: different barrier shapes and width and magnetic inductions.

IV. ANALYTICAL CALCULATION OF THE CRITICAL CURRENT AND THE SHAPE CHANGES OF A VORTEX TUNNELING THROUGH THE BARRIER

A. Qualitative estimate of the critical current from the balance of the Lorentz and the pinning forces

The critical current is defined by the condition $F_L = F_p$, where F_L is the overall Lorentz force applied by the bias current on the segment of vortex matter between two adjacent parallel barriers and F_p is the pinning force of the barrier on a line of vortices coming in contact with the stripe. The Lorentz force (per unit thickness of the film) created by the bias current drives system of the $N_x \times N_y$ vortices in physical units is

$$F_L = \frac{\Phi_0}{c} J N_x N_y. \tag{23}$$

It does not depend significantly on the distribution of either the magnetic field or the order parameter. The pinning force acting on the line of $N_y/2$ vortices of the hexagonal lattice pinned along the stripe (see Fig. 3) can be estimated as follows (see a rigorous derivation from the GL equations in the next section):

$$F_p = \frac{H_c^2}{8\pi} a N_y. \tag{24}$$

Here, the height of the energy barrier force is roughly given by the energy density associated with destruction of superconductivity in the vortex core [H_c is the thermodynamic critical field[2] $H_c = \Phi_0/(\pi 2^{3/2}\xi\lambda)$] and it varies on the scale a of order of the coherence length ξ (see Fig. 2).

The critical current condition $F_L = F_p$ therefore takes a form

$$J_c = \frac{c H_c^2}{8\pi \Phi_0} \frac{\xi}{N_x}. \tag{25}$$

By using $H_{c2} = \frac{\Phi_0}{2\pi\xi^2}$ and Eq. (10), one obtains for the dimensionless current density defined above

$$j_c = \frac{1}{32\pi^2 N_x}. \tag{26}$$

For $N_x = 16$, this gives $j_c = 1.2 \times 10^{-3}$ in qualitative agreement with the numerical simulations of the previous section where we obtained $j_c \sim 10^{-3}$ for $b = 0.5$ and width of order ξ.

B. Derivation of balance of force equation from GL theory

Within the London approach when the vortex is considered as a pointlike object, one often considers the vortex dynamics in analogy to the overdamped motion of a particle moving under influence of two forces:[2] the driving force of the external current (the Lorentz force), which is opposed by the pinning force. In numerous situations when the vortex can not be considered as a pointlike object,[7] this approach is invalid, yet the pinning force and the Lorentz forces acting on a system of vortices (described by the order parameter) can nevertheless be defined as an integral characteristic. In this section, we derive the integral equation of the balance of forces from the GL equations described above.

Let us first consider an external current smaller than j_c and times that are much larger than the microscopic relaxation time $t_{\rm GL}$. Taking a *covariant* derivative $D_i \equiv \nabla_i - iA_i$ of the GL equations (8) in the stationary case

$$\left(-\frac{1}{2}D^2 - \frac{1-t}{2} + U + \rho\right)\psi = 0, \tag{27}$$

where $\rho = |\psi|^2$ is the superfluid density, and multiplying the result by ψ^*, one arrives at

$$\psi^*\left(-\frac{1}{2}D_i D^2 + \nabla_i U + \nabla_i \rho\right)\psi + \left(-\frac{1-t}{2} + U + \rho\right)\psi^* D_i \psi = 0. \tag{28}$$

By rewriting the second term using again the (conjugate) GL equations [Eq. (27)], this equation simplifies and takes the following form:

$$-\tfrac{1}{2}\psi^*(D_i D^2\psi) + \rho\nabla_i U + \rho\nabla_i\rho + \tfrac{1}{2}(D^{*2}\psi^*)D_i\psi = 0. \tag{29}$$

To further simplify, one makes use of the commutator $[D_i, D^2] = 2i\varepsilon_{ij}bD_j$, where ε_{ij} is the antisymmetric tensor [derived from the basic commutation relation $[D_i, D_j] = i\varepsilon_{ij}b$ (see Ref. 3)] to reexpress the first term in Eq. (29):

$$\tfrac{1}{2}(D^{*2}\psi^*)D_i\psi - \tfrac{1}{2}\psi^*[(D^2 D_i + 2i\varepsilon_{ij}bD_j)\psi] + \rho\nabla_i U + \rho\nabla_i\rho = 0. \tag{30}$$

Finally, this leads to a local relation

$$\tfrac{1}{2}(D^{*2}\psi^* - \psi^* D^2)D_i\psi + \rho\nabla_i\rho - i\varepsilon_{ij}b\psi^* D_j\psi = -\rho\nabla_i U. \tag{31}$$

From this relation, one can define the overall pinning force of a barrier.

The global balance of forces is obtained by integration of Eq. (31) over a certain area S (as was discussed above, an interesting case is one period of a periodic array):

$$F_i^{\rm surf} - \frac{i}{2}\varepsilon_{ij}b\int_S d\mathbf{r}[\psi^* D_j\psi - (D_j\psi)^*\psi] = -\int_S d\mathbf{r}\,\rho\nabla_i U. \tag{32}$$

The surface terms, which can be represented as line integrals over a gradient along certain direction (not necessarily the force direction i),

$$F_i^{\rm surf} = \int_S d\mathbf{r}\nabla_j T_{ij} = \oint_\Sigma ds_j \varepsilon_{jk} T_{ik}, \tag{33}$$

$$T_{ij} = \frac{1}{4}[D_j^*\psi^* D_i\psi - \psi^* D_i D_j\psi + \text{c.c.}] + \frac{1}{2}\delta_{ij}\rho^2 \tag{34}$$

were singled out (Σ denotes the edges of the area S). Therefore, in the periodic case, where the surface terms vanish, one obtains the force balance equation

$$F_i^L = -\varepsilon_{ij}bI_j = \int d\mathbf{r}\,V(\mathbf{r})\nabla_i\rho = F_i^p, \tag{35}$$

where $I_j = \int dx\,dy\;j_i$ is an integral of the current density. By using this relation that generalizes the well-known force balance equation for pointlike (or linelike in 3D) vortices within the London approximation[2] to the case when the structure of the vortex core is important, one can obtain variational estimates of the critical current supporting the numerical solution of the GL equations presented in the previous section.

C. Narrow barrier

For a narrow barrier potential [Eq. (7)] with width w of the order of coherence length or less, the Abrikosov lattice is only slightly distorted, especially for fields not very far from H_{c2}. It was shown in Ref. 14 how to calculate the static Abrikosov solution for the hexagonal lattice as an expansion in the effective small parameter $(1-b)/6$. The first two orders are

$$\psi_A(x,y) = \left(\frac{1-b}{2\beta_A}\right)^{1/2} 3^{1/8}\sum_l e^{i}\left\{1 + \frac{\beta_6(1-b)}{2\beta_A^{3/2}\sqrt{2^6 6!}}H_6\left[b^{1/2}\left(x - \frac{\pi(2l+1)}{a_\triangle b}\right)\right]\right\} \times \exp\left\{i\left[\frac{\pi l^2}{2} + \frac{\pi(2l+1)}{a_\triangle}\left(y - \frac{a_\triangle}{4}\right)\right] - \frac{b}{2}\left[x - \frac{\pi(2l+1)}{a_\triangle b}\right]^2\right\}, \tag{36}$$

where $\beta_6 = -0.278$ and $H_n(x)$ is Hermite polynomial. The leading order is usually a good approximation, however, in our case of $b = 0.5$, the first correction can not be neglected [see Fig. 3(b)]. Here, distance between the vortices is $a_\triangle = \sqrt{2\Phi_0/3^{1/2}B} = \frac{2\pi^{1/2}}{3^{1/4}b^{1/2}}$ and $\beta_A \approx 1.16$. The narrow barrier potential certainly displaces the lattice, placing the pinned

row at distance x_p from the center of the barrier [so that the function (36) is magnetically translated[2] by x_p]. Since the barrier is narrow, there are no other vortices inside the better superconductor. The simulation shown in Fig. 3(a) demonstrates that the order parameter is represented correctly near the vortex cores although the lattice is distorted at the barrier, becoming rectangular. The theoretical value of the order parameter away from vortex cores can be improved by taking into account higher orders in the small parameter $(1-b)/2$ as in Ref. 14.

The pinning force acting on all the vortices trapped between two consequent barriers according to Eq. (35) (neglecting the distortion of the lattice by the barriers) can be written as

$$F_p(X) = -\int_{-L_x/2}^{L_x/2} dx \int_0^{L_y} dy |\psi_A(x-X,y)|^2 \frac{d}{dx} U(x), \tag{37}$$

where X is the distance of the pinned row from the center of the barrier. By performing integrations and summations with leading-order part of the static solution [Eq. (36)], one arrives at (see Appendix B for details)

$$F_p(X) = \frac{\pi b^{1/2} U_0 (1-b) w L_y}{3^{1/4}\sqrt{2}\beta_A} \theta_3' \times \left\{ \frac{\pi}{2} + \frac{2\pi}{\sqrt{3}} \frac{X}{a_\triangle}, \exp\left[-\frac{\pi}{\sqrt{3}} (1+2bw^2) \right] \right\}, \tag{38}$$

where θ_n' is derivative of the elliptic theta function.[15]

The optimal X, x_p is determined therefore from minimization of the pinning force. For $w \ll 1$ (necessary to neglect the distortion), one obtains

$$x_p = -0.219 a_\triangle = -0.59/\sqrt{b}. \tag{39}$$

The critical current is

$$j_c = \frac{F_p(x_p)}{b L_x L_y} = 0.30 \frac{U_0 (1-b) w}{b^{1/2} L_x}. \tag{40}$$

One therefore obtains linear dependence on the width of the barrier w. The approximation becomes poor at $w = 0.6$. For $b = 0.5$, $U_0 = 1$, $w = 0.3$, and $L_x = 16 a_\triangle = 61$ [the same values of parameters as in the simulation, presented in Fig. 3(a)], one obtains 1.0×10^{-3}. This should be compared with 9.1×10^{-4} obtained in simulation.

D. Pinning force on a single vortex by an interface

Let us assume that *vortex cores* are well separated. This of course does not mean that the structure of the cores is unimportant and vortices can be treated as pointlike. At large magnetic fields, this is satisfied even very close to $H_{c2}(T)$, when the distance between the vortex centers is just 2ξ (see Ref. 14). The superfluid density is approximated well by Eq. (22) [see Fig. 3(a)]. The contribution of a single vortex with the core center located at position X to the pinning force on a single vortex according to Eq. (35) can be written as

$$F_p(X) = -U_0 N_y \int_{\text{unitcell}} u(x-X) \frac{d}{dx} \rho(x,y), \tag{41}$$

where ρ is given in Eq. (22) and the potential barrier in Eq. (7). The integral over the current direction y can be extended to infinity. The maximal repulsive pinning force (with respect to the vortex position relative to the interface, X) determines the critical current. The optimal distance x_p is for $b = 0.5$, $U_0 = 1$, and $w = 1.3$ simulated in Fig. 4 is $\varepsilon = 3$ and is $x_p = -1.3$. This value and the critical current $j_c = F_p/bN_xN_y = 3 \times 10^{-3}$ are in qualitative agreement with simulation.

V. DISCUSSION AND SUMMARY

To summarize, we investigated the structure and dynamics of the current-carrying state of the vortex matter in type-II superconductors in a magnetic field with the critical temperature T_1 in the presence of an array of parallel narrow line inclusions (nanostripes) of superconducting material with a higher critical temperature T_2. It is proposed that this geometry with currently achievable stripe widths as small as the coherence length of low T_c (10−100 nm) and even high-T_c superconductors (several nm) is more effective in quenching vortex motion than the commonly used pinning by defects. In this geometry, the structure of the Abrikosov vortex cores becomes dominant. We found analytically and numerically (using a phenomenological Ginzburg-Landau approach that is particularly effective to account for the core structure at large magnetic fields) the critical current for various fields, barrier shapes, and characteristics of the inclusion material.

A typical value for such a moderately optimized system is of order of $J_c = 10^{-3} J_d$, where J_d is the depairing current of the material. For low-T_c films, this might reach $10^{10} A/m^2$ as in best samples in superconducting metals. In high-T_c materials, this option might be even more attractive since pinning by defects is ineffective. Below the critical current J_c, the flux flow halted by the barriers with the row of pinned vortices held at distance $x_p \sim \xi$ in front of each barrier (see Figs. 3 and 4). The vortex cores of this row shrink significantly and the generally regular hexagonal vortex lattice becomes denser and distorted near the barrier. These vortices are "squeezed" with core radius significantly smaller than in the bulk. This row of vortices supports all the other vortices of a segment between two barriers. We developed a Ginzburg-Landau analog and the balance-of-forces equation (between the Lorentz force and the repulsion due to inclusions) [Eq. (35)] that allows a simple estimation of the critical current and x_p for arbitrary shape of the barriers. It would be very interesting to confirm these predictions of the static current-carrying state by probing the order-parameter distribution by means of STM technique.

The dynamics of the barrier penetration for current densities larger than J_c and high magnetic fields (smaller, but of the same order of magnitude as the higher critical field H_{c2} and much higher than H_{c1}) was studied numerically and demonstrates the following picture of the soliton tunneling. The estimate of the passage time is of order $10^3 t_{\text{GL}}$, where the GL time is $\gamma\xi^2/2$ (γ, diffusion constant). For Nb film, the passage time is of order $10^{-7} s$ and much smaller for high-T_c materials. The I-V curves calculated numerically, shown in Fig. 5, are of a customary type. The barrier passage dynamics might be observable in low-T_c materials by means of dynamic STM.

Let us finally note several generalizations of the results. We have studied thin films, however, if the films are thick but still smaller than the magnetic penetration depth, there are no qualitative consequences (however, one has to use the

correct effective penetration depth). The calculations were performed for zero temperature only. For low T_c, one takes into account the temperature by modifying coherence length and penetration depth. However, if the thermal fluctuations are strong (as is the case of strongly layered high-T_c cuprates), the picture becomes essentially different. The flux creep will dominate.

ACKNOWLEDGMENTS

We appreciate the useful discussions with V. Nazarov, M. Lewkowicz, and B. Y. Zhu, and acknowledge support from the Israel Scientific Foundation. Work of B.R. was supported by MOE of R.O.C. ATU program and acknowledges the hospitality and support at Physics Department of Bar Ilan University. D.L. is supported by "the Fundamental Research Funds for the Central Universities" and National Natural Science Foudation (Grant No. 10974001).

APPENDIX A: SURFACE TERMS IN THE FORCE BALANCE EQUATION

In this appendix, we derive the expression for the surface term in the force balance equation (32). Adding the complex conjugate to the consequence of the GL equation (33) leads to

$$\frac{1}{4}[(D^{*2}\psi^* - \psi^* D^2)D_i\psi + \text{c.c.}] + \frac{1}{2}\nabla_i(\rho^2) + \frac{i}{2}b\varepsilon_{ij}(\psi D_j^*\psi^* - \psi^* D_j\psi) = -\rho\nabla_i U. \tag{A1}$$

To show that the first term is a full gradient given in Eq. (31), one makes use of the following identity:

$$(D_i g)f^* = -g D_i^* f^* + \nabla_i(g f^*) \tag{A2}$$

valid for any functions f and g. In particular, for $g = D_j^*\psi^*$ and $f^* = D_i\psi$, one obtains

$$D^{*2}\psi^* D_i\psi = -D_j^*\psi^*(D_j D_i\psi) + \nabla_j(D_j^*\psi^* D_i\psi), \tag{A3}$$

and for $g = D_j D_i\psi$ and $f^* = \psi^*$,

$$\psi^*(D^2 D_i\psi) = -(D_j D_i\psi)D_j^*\psi^* + \nabla_j(\psi^* D_i D_j\psi). \tag{A4}$$

By substituting Eqs. (A3) and (A3) into Eq. (A1), one gets

$$\tfrac{1}{4}[\nabla_j(D_j^*\psi^* D_i\psi - \psi^* D_i D_j\psi) + \text{c.c.}] + \tfrac{1}{2}\nabla_i(\rho^2) + b\varepsilon_{ij}j_j = -\rho\nabla_i U. \tag{A5}$$

As a result, the force balance equation is obtained with full gradients leading to the surface terms (32).

APPENDIX B: PINNING FORCE ON THE VORTEX LATTICE

In this appendix, we provide details of calculation of the critical current for a narrow barrier. The gradient of the superfluid density of the Abrikosov lattice [Eq. (36)] shifted by X along the direction x (perpendicular to current) and integrating over the Gaussian barrier [Eq. (7)] is

$$S_1 = \int_{x,y}\rho(x,y)\frac{d}{dx}u(x) = -\frac{3^{1/4}}{2\beta_A}\frac{(1-b)b^{1/2}}{w^2} \times \int_{x,y} x\sum_{l,l'} e^{i\pi(l^2-l'^2)/2}\exp\left\{i\left[\frac{2\pi(l-l')}{a_\triangle}\left(y-\frac{a_\triangle}{4}\right)\right] - \frac{b}{2}\left[x+X-\frac{\pi(2l+1)}{a_\triangle b}\right]^2 - \frac{b}{2}\left[x-\frac{\pi(2l'+1)}{a_\triangle b}\right]^2 - \frac{x^2}{2w^2}\right\}. \tag{B1}$$

Integration over y helps to sum over l':

$$S_1 = -\frac{3^{1/4}}{2\beta_A}\frac{L_y(1-b)b^{1/2}}{w^2}\sum_l\int_x x\exp\left\{-b\left[x+X-\frac{\pi(2l+1)}{a_\triangle b}\right]^2 - \frac{x^2}{2w^2}\right\}. \tag{B2}$$

By integrating over x, one obtains the sum

$$S_1 = -\frac{3^{1/4}\sqrt{2\pi}}{\beta_A}\frac{b^{3/2}(1-b)wL_y}{(1+2bw^2)^{3/2}}\sum_l\left[\frac{\pi(2l+1)}{a_\triangle b}+X\right]\exp\left\{-\frac{b}{1+2bw^2}\left[\frac{\pi(2l+1)}{a_\triangle b}+X\right]^2\right\}. \tag{B3}$$

Differentiating the elliptic theta function representation (see Ref. 15)

$$s_0 = \sum_l\exp\{-\alpha[\varepsilon(2l+1)+X]^2\} = \frac{\sqrt{\pi/\alpha}}{2\varepsilon}\theta\left[3,\frac{\pi}{2}\left(1+\frac{X}{\varepsilon}\right),\exp\left(-\frac{\pi^2}{4\alpha\varepsilon^2}\right)\right] \tag{B4}$$

with respect to X, one obtains an identity

$$\frac{ds_1}{dx_0} = -2\alpha\sum_l[\varepsilon(2l+1)+X]\exp\{-\alpha[\varepsilon(2l+1)+X]^2\} = -\frac{\pi^{3/2}}{8\varepsilon^2\alpha^{3/2}}\theta'\left[3,\frac{\pi}{2}\left(1+\frac{X}{\varepsilon}\right),\exp\left(-\frac{\pi^2}{4\alpha\varepsilon^2}\right)\right], \tag{B5}$$

which allows (identifying $\alpha = \frac{b}{1+2bw^2}$ and $\varepsilon = \frac{\pi}{a_\triangle b} = \frac{3^{1/4}\pi^{1/2}}{2b^{1/2}}$) the elliptic function representation of the pinning integral

$$S_1 = \frac{\pi}{3^{1/4}\sqrt{2}\beta_A} b(1-b) w L_y \theta' \left[3, \frac{\pi}{2}\left(1 + \frac{X}{\varepsilon}\right), \exp\left(-\frac{\pi^2}{4\alpha\varepsilon^2}\right)\right] \tag{B6}$$

from which Eq. (38) follows.

[1] N. Kopnin, Vortices in type-II superconductors: Structure and Dynamics (Oxford University Press, Oxford, 2011).

[2] G. Blatter, M. V. Feigelman, V. B. Geshkenbein, A. I. Larkin, and V. M. Vinokur, Rev. Mod. Phys. **66**, 1125 (1994).

[3] B. Rosenstein and D. P. Li, Rev. Mod. Phys. **82**, 109 (2010).

[4] R. Prozorov, M. Konczykowski, B. Schmidt, Y. Yeshurun, A. Shaulov, C. Villard, and G. Koren, Phys. Rev. B **54**, 15530 (1996); N. Avraham, Y. Y. Goldschmidt, J. T. Liu, Y. Myasoedov, M. Rappaport, E. Zeldov, C. J. van der Beek, M. Konczykowski, and T. Tamegai, Phys. Rev. Lett. **99** 087001 (2007); M. Weigand, M. Eisterer, E. Giannini, and H. W. Weber, Phys. Rev. B **81**, 014516 (2010).

[5] M. Montero, O. Stoll, and I. Schuller, Europhys. J. B **40**, 459 (2004); A. A. Zhukov, E. T. Filby, P. A. J. de Groot, V. V. Metlushko, and B. Ilic, Physica C **404**, 166 (2004); U. Welp, Z. L. Xiao, V. Novosad, and V. K. Vlasko-Vlasov, Phys. Rev. B **71**, 014505 (2005); J. E. Villegas, E. M. Gonzalez, Z. Sefrioui, J. Santamaria, and J. L. Vicent, *ibid.* **72**, 174512 (2005); Q. H. Chen, G. Teniers, B. B. Jin, and V. V. Moshalkov, *ibid.* **73**, 014506 (2006); J. E. Villegas, M. I. Montero, C.-P. Li, and I. K. Schuller, Phys. Rev. Lett. **97**, 027002 (2006); A. Yu. Aladyshkin, A. V. Silhanek, W. Gillijns, and V. V. Moshchalkov, Supercond. Sci. Technol. **22**, 053001 (2009); H. Q. Nguyen, S. M. Hollen, M. D. Stewart, J. Shainline, Aijun Yin, J. M. Xu, and J. M. Valles, PRL **103**, 157001 (2009).

[6] J. Eisenmenger, P. Leiderer, M. Wallenhorst, and Horst Dötsch, Phys. Rev. B **64**, 104503 (2001); C. W. Luo, C. C. Lee, C. H. Li, H. C. Shih, Y.-J. Chen, C. C. Hsieh, C. H. Su, W. Y. Tzeng, K. H. Wu, J. Y. Juang, T. M.Uen, S. P. Chen, J.-Y. Lin, and T. Kobayashi, Opt. Express **16**, 20610 (2008).

[7] B. Rosenstein, I. Shapiro, and B. Ya. Shapiro, Phys. Rev. B **83**, 064512 (2011).

[8] D. R. Nelson and V. M. Vinokur, Phys. Rev. B **48**, 13060 (1993); M. C. Marchetti and V. M. Vinokur, Phys. Rev. Let. **72**, 3409 (1994).

[9] L. Burlachkov, I. B. Khalfin, and B. Ya. Shapiro, Phys. Rev. B **48**, 1156 (1993).

[10] C. H. Ahn, J. M. Triscone, and J. Mannhart, Nature **424**, 1015 (2003).

[11] D. Li, A. M. Malkin, and B. Rosenstein, Phys. Rev. B **70**, 214529 (2004); B. Rosenstein and V. Zhuravlev, *ibid.* **76**, 014507 (2007).

[12] D. J. Priour and H. A. Fertig, Phys. Rev. B **67**, 054504 (2003); B. Rosenstein, I. Shapiro, and B. Ya. Shapiro, *ibid.* **81**, 064507 (2010).

[13] W. D. Gropp, H. G. Kaper, G. K. Leaf, D. M. Levine, M. Palumbo, and V. M. Vinokur, J. Comp. Phys. **123**, 254 (1996); G. R. Berdiyorov, M. V. Milošević, and F. M. Peeters, Phys. Rev. B **74**, 174512 (2006); G. R. Berdiyorov, A. K. Elmurodov, F. M. Peeters, and D. Y. Vodolazov, *ibid.* **79**, 174506 (2009); A. N. Zotova and D. Y. Vodolazov, *ibid.* **85**, 024509 (2012).

[14] D. Li and B. Rosenstein, Phys. Rev. B **60**, 9704 (1999); T. Maniv, B. Rosenstein, I. Shapiro, and B. Ya. Shapiro, *ibid.* **80**, 134512 (2009).

[15] I. S. Gradshteyn and L. M. Ryzhik, *Table of Integrals, Series, and Products*, 6th ed. (Elsevier, Singapore, 2004).